ROTORDYNAMIC FORCES ON A THREE BLADED INDUCER UNDER FORCED WHIRL MOTION OPERATING AT DIFFERENT CONDITIONS

Dario Valentini[1♥], Giovanni Pace[1*], Lucio Torre[2♣], Angelo Pasini[2⋐] and Luca d'Agostino[1♦]

[1]University of Pisa, Civil and Industrial Engineering Department
2 Largo Lucio Lazzarino, Pisa, 56126, Italy
♥d.valentini@alta-space.com *g.pace@alta-space.com ♦luca.dagostino@ing.unipi.it

[2]ALTA S.p.A.
5 Via Gherardesca, Ospedaletto, Pisa, 56121, Italy
♣l.torre@alta-space.com ⋐a.pasini@alta-space.com

Abstract

The paper illustrates the main results of an experimental campaign conducted in the CPRTF (Cavitating Pump Rotordynamic Test Facility) at ALTA S.p.A., aimed at characterizing the rotordynamic forces acting on a whirling three-bladed, tapered-hub, variable-pitch inducer, named DAPROT3. The forces acting on the impeller have been measured by means of a rotating dynamometer mounted just behind the inducer. The roles of the imposed whirl motion of the rotor, flow coefficient, cavitation number and liquid temperature have been investigated. The results have been obtained by means of a recent experimental technique, consisting in measuring the continuous spectra of the rotordynamic forces as functions of the whirl excitation frequency. This technique allows for extrapolating valuable information from the experiments by more accurately and rapidly characterizing the spectral behavior of these forces than can be obtained from a limited number of point experiments conducted at constant whirl frequency. Therefore, it is useful to better capture the complexity of the rotordynamic forces and assess their consequences on the stability of axial inducers.

Introduction

Rotordynamic forces, together with flow instabilities eventually triggered by cavitation, are one of the most recognized and dangerous sources of vibrations in turbomachines ([1][2][3][4]). These forces can affect all the components of the machine, including the bearings, the seals and, obviously, the impeller itself ([5]).
Even if steady and rotordynamic forces acting on centrifugal pump impellers have been extensively investigated (see for example [6] -[7]), the influence of cavitation on rotordynamic fluid forces has not yet been investigated in great detail. Available experimental data mainly come from the work carried out at the California Institute of Technology, (in particular see [8] -[1]). Up to the present date, the most complete set of experimental data reported in open literature for axial inducers are those by Bhattacharyya ([2],[1]) and by the Chemical Propulsion Team at ALTA S.p.A. ([9] -[10]).
Recently, in the framework of a project funded by the European Space Agency, an experimental campaign has been carried out at ALTA S.p.A. on a three bladed axial inducer aimed at investigating the influence on rotordynamic forces of:

- (inertial/thermal) cavitation;
- flowrate;
- flow temperature (inertial/thermal cavitation).

In the experiments the impeller is subject to a whirl motion of given constant eccentricity and angular velocity. A special procedure ([9]), recently developed and validated at ALTA S.p.A., has been used to measure the continuous spectrum of rotordynamic forces as functions of the whirl-to-rotational speed ratio. This procedure proved to be very effective in providing accurate and frequency-resolved information on how rotordynamic forces depend on the whirl ratio. In particular, the maxima and minima of such forces can be clearly identified, together with the general trend of their spectral behavior.

Nomenclature

$\boldsymbol{A}$	rotordynamic matrix
A_{ij}	element of the rotordynamic matrix
c_a	full-blade axial length
F	generalized dimensional force
F^*	generalized nondimensional force
L	axial length
p	static pressure
Q	volumetric flow rate
r_H	inducer hub radius
r_T	inducer tip radius
T	temperature
ε	radius of the whirl orbit (eccentricity)
ρ	liquid density
σ	Euler number $\sigma = \left(p_1 - p_v\right)/0.5\rho\Omega^2 r_T^2$

Φ	flow coefficient $\Phi = Q/\pi\Omega r_T^3$
ϕ	phase of the rotordynamic force
ω	whirl rotational speed
Ω	inducer rotational speed

Subscripts

D	design conditions
N	normal to the whirl orbit/ nominal
R	rotordynamic force modulus
T	tangent to the whirl orbit
H	hub radius
x, y	rotating reference frame
X, Y	absolute reference frame
t	total
le	blade leading edge
te	blade trailing edge
v	vapor pressure
0	initial condition/ steady forces

Experimental Apparatus

Test Facility and Instrumentation

The experimental activity reported in the present paper has been carried out in ALTA's Cavitating Pump Rotordynamic Test Facility (CPRTF), illustrated in Figure 1 and specifically designed for characterizing the performance of cavitating and/or noncavitating turbopumps in a wide variety of alternative configurations (axial, radial or mixed flow, with or without an inducer ([11],[12]). The facility uses water as working fluid at temperatures up to 90 °C and is intended as a flexible apparatus readily adaptable to conduct experimental investigations on virtually any kind of fluid dynamic phenomena relevant to high performance turbopumps. The pump housing and the inlet section can be easily adapted to host machines and inducers with actual geometries of different sizes. Unsteady pressure sensors can be flush-mounted on the casing walls of the pump to detect, identify and monitor the occurrence of flow instabilities developing in the machine.

The facility is instrumented with a series of transducers for measuring:

- the inducer inlet pressure;
- the inducer static pressure rise;
- the pressure fluctuations, in order to identify the presence of flow instabilities;
- the volumetric flow rate on the suction line;
- the volumetric flow rate on the discharge line;
- the fluid temperature inside the main tank;
- the absolute angular position of the driving shaft;
- the absolute angular position of the eccentric shaft which generates the whirl motion.

Figure 1. The cavitating pump rotordynamic test facility.

A rotating dynamometer in the test section allows for the measurement of the forces and moments acting on the impeller. The generation of the eccentricity is realized by means of a two-shafts mechanism. The shafts are assembled one inside the other by means of a double eccentric mount and their eccentricity can be finely adjusted from 0 and 2 mm by changing the relative angular position of the double eccentric mount before each test. The whirl motion is generated by a brushless motor driving the external shaft, while the impeller rotation is imparted by connecting the internal shaft to the main motor with an omokinetic coupling.

The rotating dynamometer for the measurement of rotordynamic forces and moments is realized in one single piece of phase hardening steel AISI 630 H1025 and consists of two flanges connected by four square cross-section posts acting as flexible elements. The deformation of the posts is measured by 40 semiconductor strain gauges arranged in 10 full Wheatstone bridges, which provide redundant measurements of the forces and moments acting on the impeller. Each bridge is temperature self-compensated, with separate bipolar excitation and read-out for better reduction of cross-talking. The sizing of the sensing posts is the result of a trade-off between sensitivity and structural resistance, operational stability and position control (stiffness). The current design of the dynamometer is optimized for a suspended mass of 4 kg with 70 mm gyration radius, an added mass of about 2 kg (based on the expected magnitude of the rotordynamic forces), a rotational speed of 3000 rpm without eccentricity, and maximum rotational and whirl speeds up to 2000 rpm with 2 mm shaft eccentricity.

Figure 2 shows a rendering of the test chamber assembly used for the experimental campaign reported in the present paper. The rotating dynamometer is placed between the inducer and the driving shaft. The inducer is therefore suspended for the measurement of the rotor forces. In order to reduce cantilever effects of the impeller shaft, the inducer has been recessed with respect to the optical access to the test section inlet. In this configuration the inducer blades are contained within the "inlet duct". A nominal clearance of 2 mm has been selected in order to accommodate sufficiently large whirl eccentricities for generating measurable rotordynamic forces without excessively increasing tip leakage effects. The inducer is connected to the dynamometer by means of a male/female conical adapter. A screwed component is coupled on one side with a threaded hole

machined in the conical interface of the dynamometer and on the other side with a retaining nut.

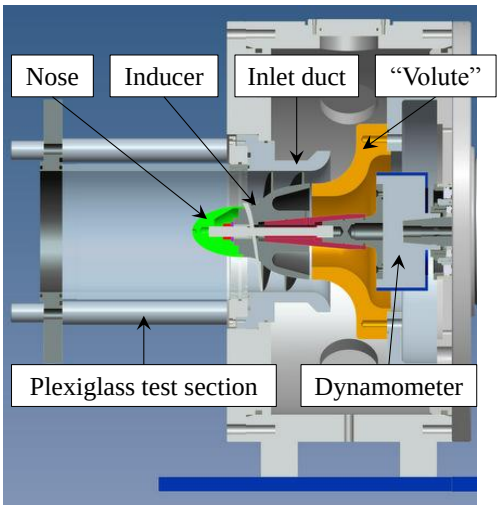

Figure 2. Rendering of the test chamber assembly.

The relative positions of the inducer on the adapter and of the adapter on the dynamometer interface are guaranteed by means of two pins. The "volute" has been mounted on the test section in order to reduce the suspended mass and minimize the interference with the measurement of the forces acting on the inducer. In order to avoid water sloshing effects in the inducer assembly (for example within the nose) the upstream nose and the conical mounts of the inducer have been sealed by means of o-rings.

Test Article

The test item, manufactured in 7075-T6 aluminum alloy, is a three-bladed, tapered-hub, variable-pitch inducer named DAPROT3 (Figure 3). The test inducer, whose main geometrical and operational data are reported in Table 1, has been designed by means of the reduced order model described in[13], [14].

Suitable settings for the inputs of the model allow for designing an inducer with dimensions fully compatible with the CPRTF configuration. A reasonable value of the blade loading (with a diffusion factor D = 0.47 as defined in[13], [14]) and a solidity σ_T = 1.68 have been chosen for reducing the leading-edge cavity and improving the suction performance. The value of the tip incidence-to-blade angle ratio α/β_b < 0.5 has been selected with the aim of controlling the danger of surge instabilities at design flow under cavitating conditions.

Figure 3. The DAPROT3 inducer.

Table 1. Geometrical and operational parameters of the DAPROT3 inducer.

Design flow coefficient	[--]	Φ_D	0.065
Number of blades	[--]	N	3
Tip radius	mm	r_T	81.0
Inlet tip blade angle	deg	γ_{Tle}	82.10
Inlet hub radius (fully-developed blade)	mm	r_{Hle}	44.5
Outlet hub radius	mm	r_{Hte}	65.6
Mean blade height	mm	h_m	25.95
Axial length (fully-developed blade)	mm	c_a	63.5
Inlet hub radius	mm	r_{H1}	35.0
Axial length	mm	L	90.0
Diffusion factor	[--]	D	0.47
Ratio tip incidence / blade angles	[--]	α/β_b	0.33
Tip solidity	[--]	σ_T	1.68
Incidence tip angle @ design	deg	α	2.58
Outlet tip blade angle	deg	γ_{Tte}	70.56

Experimental Procedure

A circular whirl orbit has been imposed to the DAPROT3 impeller in order to determine the corresponding fluid-induced rotordynamic forces. The generic components of the instantaneous forces acting on a whirling inducer are schematically shown in Figure 4. The instantaneous force vector $\vec{F}$ can be expressed as the sum of a steady force $\vec{F}_0$ (not depending on the rotor eccentricity) and an unsteady force generated by the eccentricity vector $\vec{\varepsilon}$ and represented by means of the rotordynamic matrix $\boldsymbol{A}$:

$$\begin{pmatrix} F_X \\ F_Y \end{pmatrix} = \begin{pmatrix} F_{0X} \\ F_{0Y} \end{pmatrix} + \begin{bmatrix} A_{XX} & A_{XY} \\ A_{YX} & A_{YY} \end{bmatrix} \begin{pmatrix} \varepsilon\cos(\omega t + \omega_0) \\ \varepsilon\sin(\omega t + \omega_0) \end{pmatrix}$$

where ω_0 is the anomaly of the eccentricity at the initial acquisition time t_0. Since the rotordynamic matrix $\boldsymbol{A}$ expresses a (rotational) transformation between two coplanar vectors, its elements satisfy the symmetry conditions $A_{XX} = A_{YY}$ and $A_{XY} = -A_{YX}$.

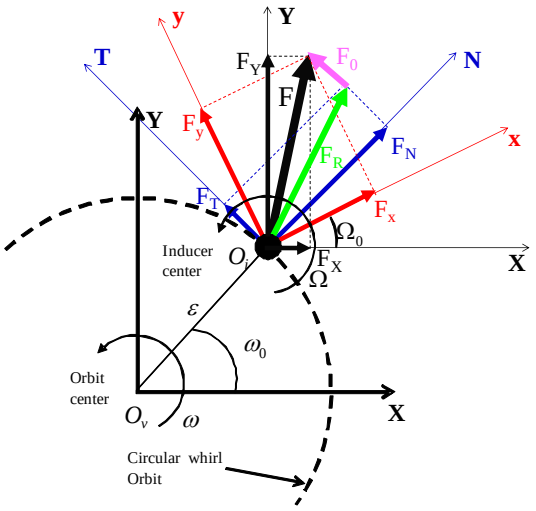

Figure 4. Schematic representation of the rotordynamic forces in the laboratory and rotating reference frames.

The normal and tangential forces with respect to the whirl orbit, F_N and F_T, can be expressed as:

$$F_N = \frac{1}{2}\left(A_{XX} + A_{YY}\right) = A_{XX} = A_{YY}$$

$$F_T = \frac{1}{2}\left(A_{YX} - A_{XY}\right) = -A_{XY} = A_{YX}$$

The normal force F_N is assumed positive when in the outward direction, while F_T is positive if it has the same direction of the impeller rotational speed Ω. Therefore the normal force is destabilizing when positive (tending to increase the magnitude of the eccentricity) and stabilizing when negative. Similarly, the tangential force is destabilizing when has the same sign as the whirl speed (promoting the rotation of the eccentricity) and stabilizing when the reverse is the case. It is worth noting once more that the data presented in this paper only refer to the fluid forces induced by the rotor eccentricity. The effects of gravity, buoyancy and tare forces (the submerged weight and the centrifugal force generated by the whirl motion on the rotor mass), as well as the steady fluid force on the impeller (like those induced by azimuthal asymmetries of the flow), have been subtracted from the total force read by the dynamometer. The rotordynamic forces have been normalized as follows ([2],[1]):

$$F_N^* = \frac{F_N}{\pi\rho c_a \varepsilon \Omega^2 r_T^2} \qquad F_T^* = \frac{F_T}{\pi\rho c_a \varepsilon \Omega^2 r_T^2}$$

where ρ is the fluid density, c_a is the axial length of the inducer blades, ε is the radius of the whirl orbit (eccentricity), Ω is the inducer rotational speed and r_T is the inducer tip radius.

Two different approaches have been used to evaluate the spectral dependence of rotordynamic fluid forces on the whirl speed. The first "traditional" approach consists in the evaluation of the rotordynamic forces from separate experiments carried out at discrete values of the whirl ratio ω/Ω (see [10],[15]). The second procedure, illustrated in detail in a previous paper ([9]), obtains a continuous measurement of the rotordynamic force spectrum as a function of the whirl ratio from the data acquired in a single experiment with an imposed variation of the whirl speed.

Test matrix

The experimental campaign carried out on the DAPROT3 inducer has been aimed at understanding how the rotordynamic forces are influenced by:

- the inducer flow coefficient;
- the occurrence of cavitation;
- the fluid temperature (inertial/thermal cavitation).

All tests have been carried out with whirl eccentricity ε = 1.130 mm and impeller rotational speed Ω = 1750 rpm, which represent a suitable compromise between the generation of measurable rotordynamic forces and the structural integrity of the rotating dynamometer under the resulting centrifugal forces on the rotor. Only sub-synchronous whirl ratios have been investigated, with both positive and negative values up to ±0.7 (ω/Ω = ±0.1, ±0.3, ±0.5, ±0.7 for the discrete approach). Eighteen different combinations of flow rate, cavitation conditions and water temperature have been considered, as summarized in the test matrix of Table 2.

Table 2. Test matrix.

Φ	σ_N	T
0.052 (0.8 Φ_D)	1.015	20 °C
		70 °C
	0.143	20 °C
		70 °C
	0.088	20 °C
		70 °C
0.065 (Φ_D)	1.015	20 °C
		70 °C
	0.143	20 °C
		70 °C
	0.088	20 °C
		70 °C
0.078 (1.2 Φ_D)	1.015	20 °C
		70 °C
	0.143	20 °C
		70 °C
	0.088	20 °C
		70 °C

The effect of the flow rate on the rotordynamic forces has been studied at three flow coefficients (Φ = 0.052, Φ = 0.065 and Φ = 0.078), corresponding respectively to 80%, 100% and 120% of the design flow coefficient. Three (nominal) values of the Euler number σ_N have been selected in order to obtain different cavitating conditions: noncavitating (σ_N = 1.015), (σ_N = 0.143) and highly cavitating (σ_N = 0.088).

Finally all the tests have been performed at two different water temperatures: 20 °C and 70 °C (±0.5 °C).

Results and Discussion

Noncavitating Performance and Hydraulic Efficiency

A series of tests has been conducted on the DAPROT3 inducer in order to characterize its noncavitating pumping performance and hydraulic efficiency at 20 °C in the same nominal (zero eccentricity) configuration (2 mm blade tip clearance, corresponding to 7.7% of the mean blade height) used in rotordynamic tests.

Figure 5 shows the noncavitating experimental curves in terms of the head coefficient $Y = Dp / r W^2 r_T^2$ and total-to-total hydraulic efficiency $h = Q Dp_t / (t W)$ as functions of the flow coefficient $F = Q / pW r_T^3$.

The volumetric flow rate (Q) has been measured by means of an electromagnetic flowmeter (mod. 8732E by Fisher-Rosemount, range 0–100 l/s, 0.5% precision) mounted on the discharge line, the static pressure increase (Δp) by means of a differential pressure transducer (Druck, model PMP 4170, 0÷1 bard operating range, 0.08% precision class). The low pressure tap has been located on the suction line about 6 inducer diameters upstream of the blade leading edges, in order to eliminate the effect of inlet flow prerotation. The high pressure tap has been mounted on the discharge line at about 2.5 duct diameters downstream of the test chamber connection, because of the uncertainties in compensating for the influence of exit flow swirl if mounted on the inducer discharge casing. Hence head measurements include the (negligible) viscous losses from the upstream pressure tap to the inducer inlet, as well as the diffusion losses from the inducer outlet into the test section and the entrance losses in the discharge line. In order to evaluate the total pressure rise, two main assumptions have been made according to the model explained in detail in a previous paper ([15]):

- the static pressure in the discharge line is equal to the bulk static pressure at the exit of the inducer;
- the azimuthal velocity at the inducer exit can be evaluated by means of the Carter's rule.

The torque (τ) has been directly measured by means of the rotating dynamometer, thereby by-passing the uncertainties associated with seal friction on the inducer shaft.

The maximum measured efficiency (about 82%) corresponds to a flowrate close to the design flow coefficient (Φ = 0.065), in accordance with the typical optimization made for this kind of machine.

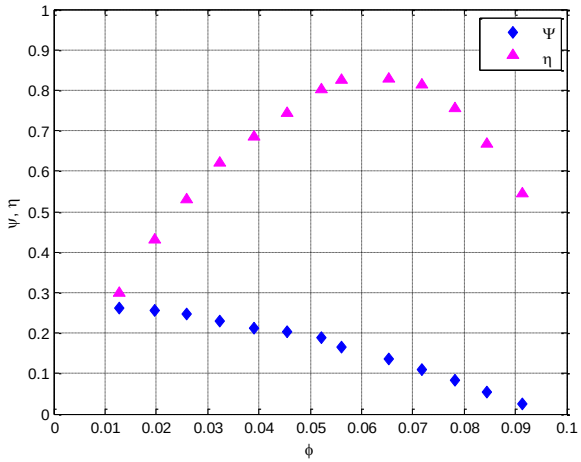

Figure 5. Noncavitating pumping performance and hydraulic efficiency curves of the DAPROT3 inducer.

Rotordynamic Forces

In the following, the rotordynamic forces are reported both in terms of F_N^* , F_T^* , their non-dimensional modulus $\left|\vec{F}_R^*\right| = \sqrt{\left(F_N^*\right)^2 + \left(F_T^*\right)^2}$, and the phase angle ϕ as functions of the whirl ratio ω/Ω. Recalling that these forces are to be considered destabilizing when they tend to increase the whirl eccentricity or sustain its rotation, the normal component is therefore destabilizing when directed outward, while the tangential component is destabilizing when directed in the same direction as the whirl motion. Figures 6-7 show as green, yellow, orange and red areas the stability regions for positive and negative whirl ratios.

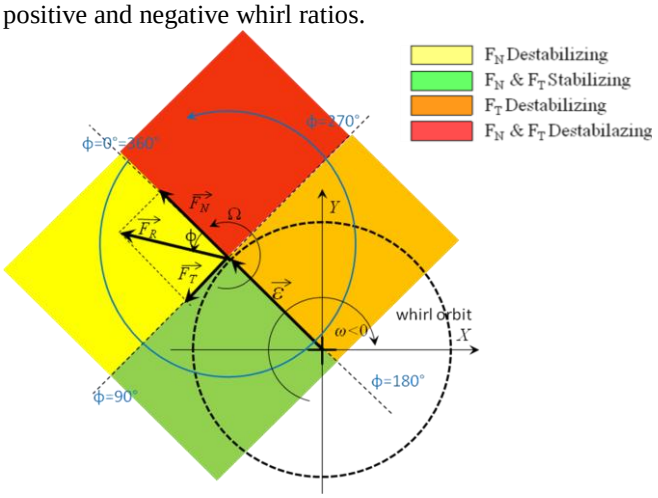

Figure 6. Stability regions of the normal and tangential components of the rotordynamic force for negative whirl ratios.

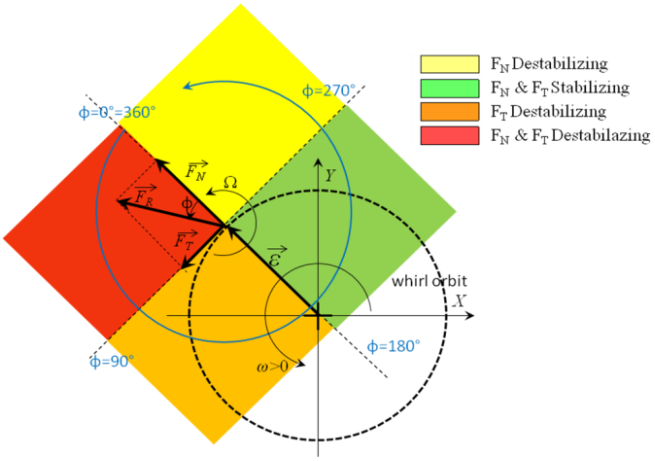

Figure 7. Stability regions of the normal and tangential components of the rotordynamic force for positive whirl ratios.

The most representative results obtained under the conditions described in Table 2 are presented in the figures 8-21. The continuous spectra of the forces are of particular interest as they provide a general overview of how the rotordynamic force depends on the whirl ratio and allow for clear identification of the maxima and minima of the curves.

As shown by all of the figures, the continuous spectra almost perfectly match the discrete results obtained by means of the classical data reduction procedure. Furthermore, continuous experiments simplify the experimental procedure allowing for the collection of all the necessary data in only two experimental sessions, one for positive whirl ratios and the other for negative ones. On the other hand, each discrete result is obtained in one experimental session and, consequently, the test procedure is much longer and complicated.

Figures 8 and 9 show the effect of the flow coefficient under noncavitating cold flow condition. The influence of the flow coefficient can be clearly identified in some concomitant effects on the rotordynamic force that are in a very good agreement with the effects detected in other inducers tested in previous experiments ([13]). The first effect is that the lower the flow coefficient, the higher the intensity of the rotordynamic force. At the same time there is a general trend for the maxima and minima to shift towards higher values of the whirl ratio as the flow coefficient decreases.

For the nominal and highest flow coefficient the normal component of the rotordynamic force shows a parabolic behavior very similar to the typical one obtained for centrifugal impellers ([16]). On the other hand, at the lowest flowrate this trend is manifest only for negative whirl. At all flowrates the normal component of the rotordynamic force becomes destabilizing for whirl ratios $\omega/\Omega \leq -0.3$. The lowest flow coefficients are generally associated to a more stabilizing behavior of both the normal and tangential components of the rotordynamic force.

Generally, the intensity of the rotordynamic force displays a both minimum and a maximum for positive whirl ratios. As shown by the phase chart (figure 9), the minimum corresponds to a sudden variation of the angular phase, while the maximum takes place when the rotordynamic force becomes destabilizing.

Figures 10-13 show the comparison of the rotordynamic force spectra corresponding to different values of the flow coefficient for cold water tests (T = 20 °C) at the remaining two cavitation numbers (σ_N = 0.143, σ_N = 0.088). The general influence of the flow coefficient is confirmed also under both slight and intense cavitation conditions.

Figures 14-19 show the effect of varying the cavitation conditions at fixed values of the flow coefficient (Φ = 0.052, Φ = 0.065, Φ = 0.078) and fluid temperature (T = 20 °C). For the lowest flow coefficient, the effect of the cavitation is clearly negligible, while at higher flow coefficients the influence of cavitation tends to increase. When cavitation starts to influence the rotordynamic forces, its effects tend to increase the intensity of the rotordynamic force, especially at lower Euler numbers (figures 18, 19). Moreover, the destabilizing behavior of the normal component is delayed by the presence of cavitation in the range of whirl ratios from ω/Ω = –0.3 to ω/Ω = –0.5 (see Figure 18).

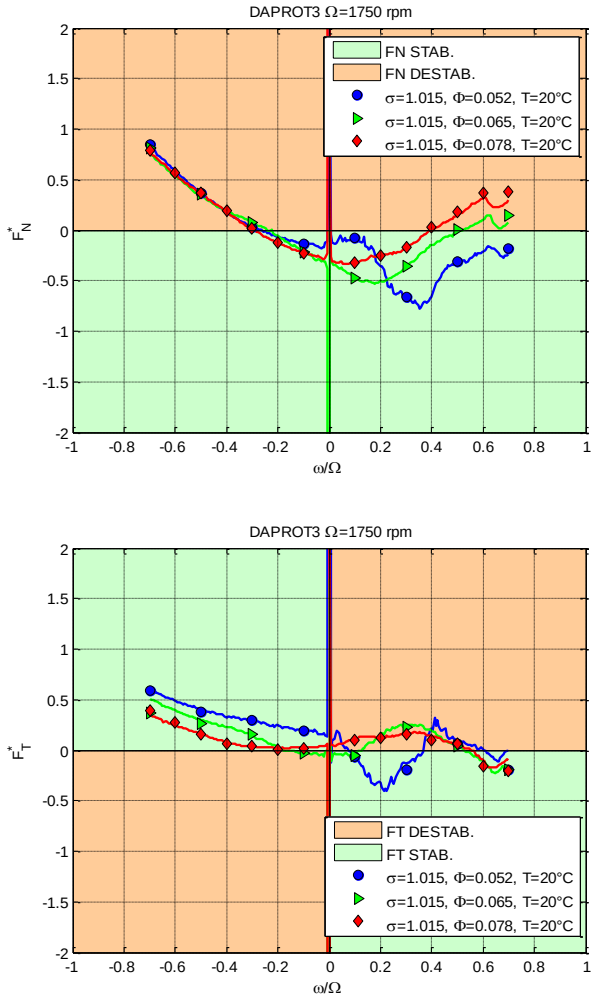

Figure 8. Effect of the flow coefficient on the normal and tangential components of the rotordynamic force (cold test at σ_N = 1.015).

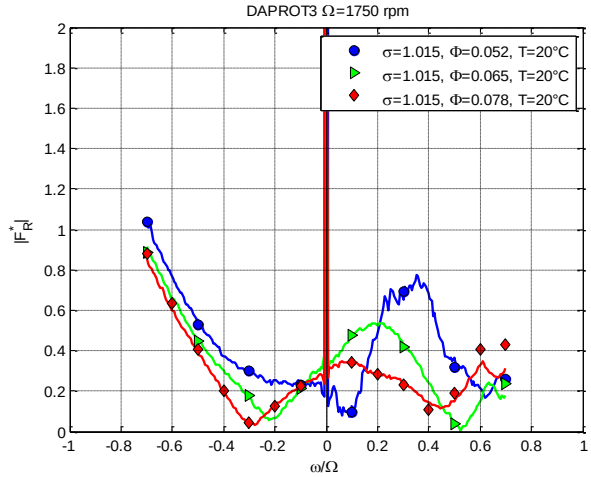

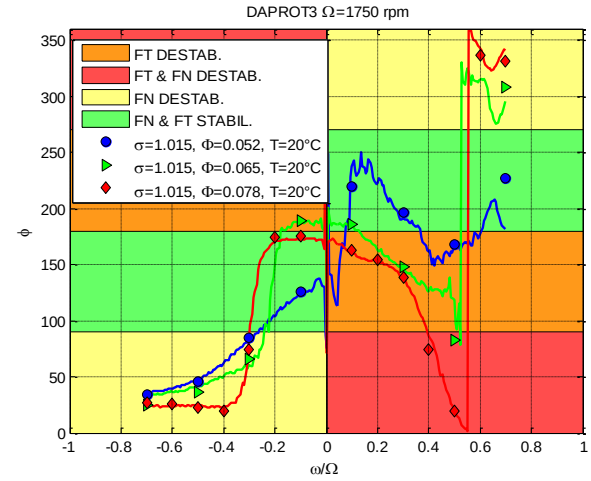

Figure 9. Effect of the flow coefficient on the intensity and phase of the rotordynamic force (cold test at $\sigma_N = 1.015$).

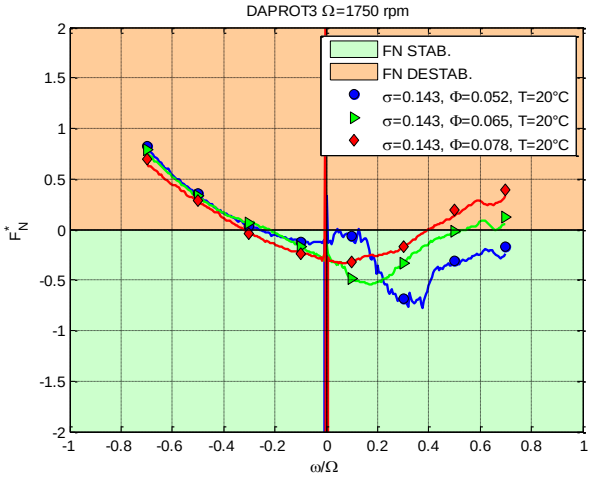

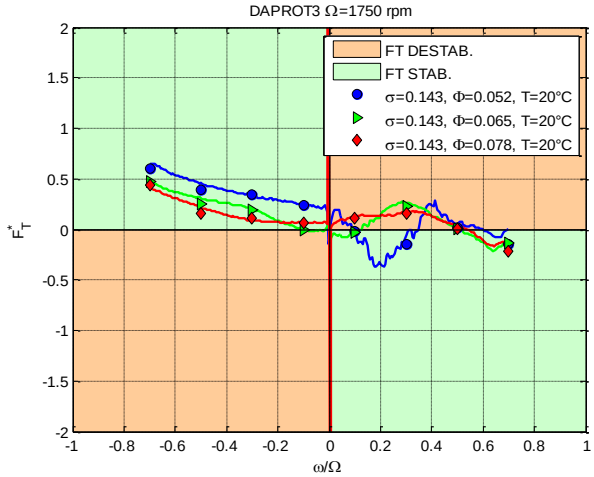

Figure 10. Effect of the flow coefficient on the normal and tangential components of the rotordynamic force (cold test at $\sigma_N = 0.143$).

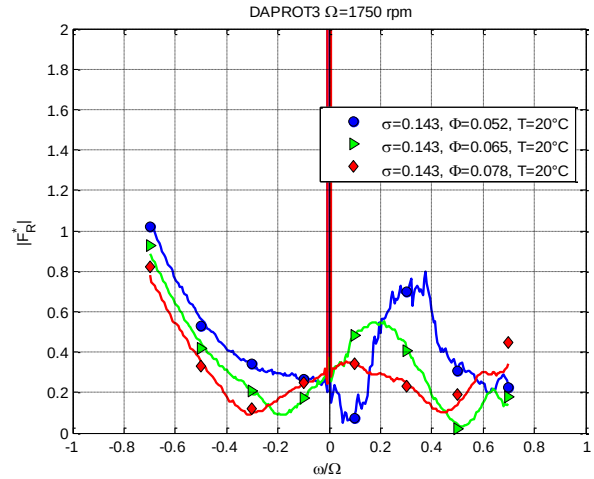

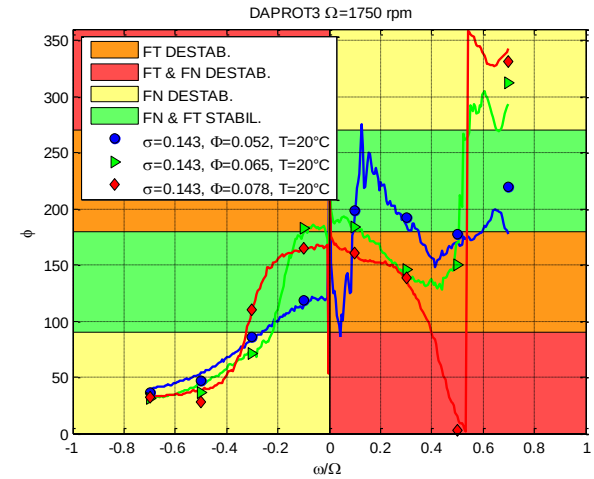

Figure 11. Effect of the flow coefficient on the intensity and phase of the rotordynamic force (cold test at $\sigma_N = 0.143$).

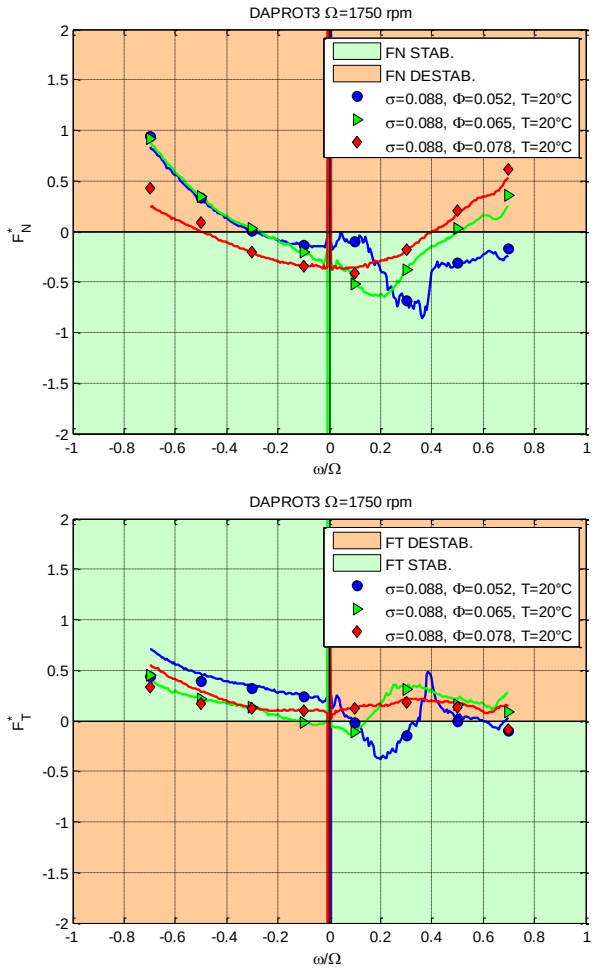

Figure 12. Effect of the flow coefficient on the normal and tangential components of the rotordynamic force (cold test at σ_N = 0.088).

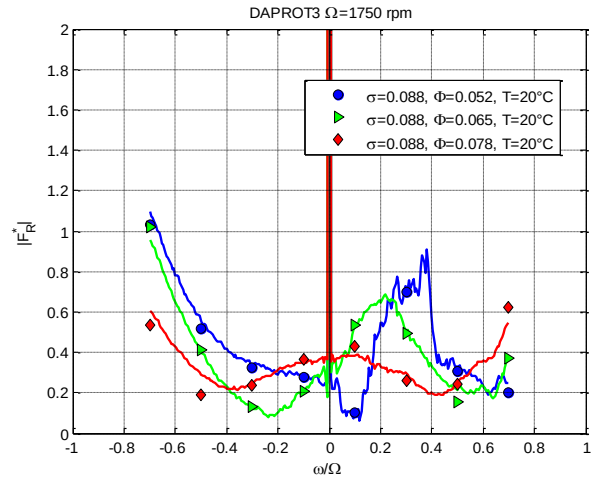

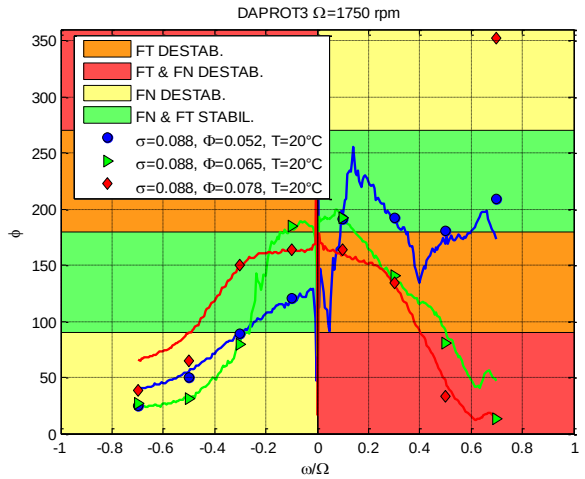

Figure 13. Effect of the flow coefficient on the intensity and phase of the rotordynamic force (cold test at σ_N = 0.088).

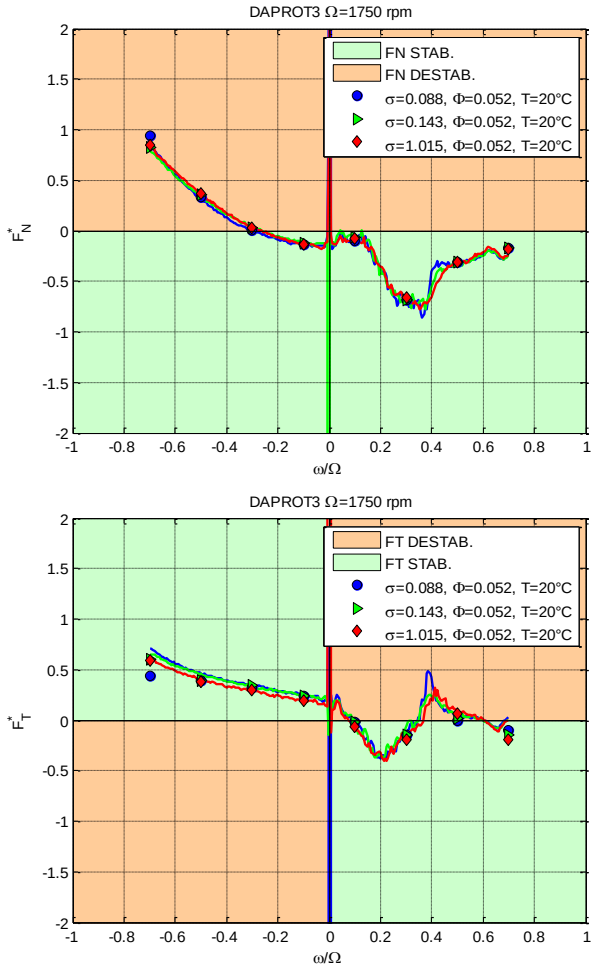

Figure 14. Effect of the cavitation number on the normal and tangential components of the rotordynamic force (cold test at Φ = 0.052).

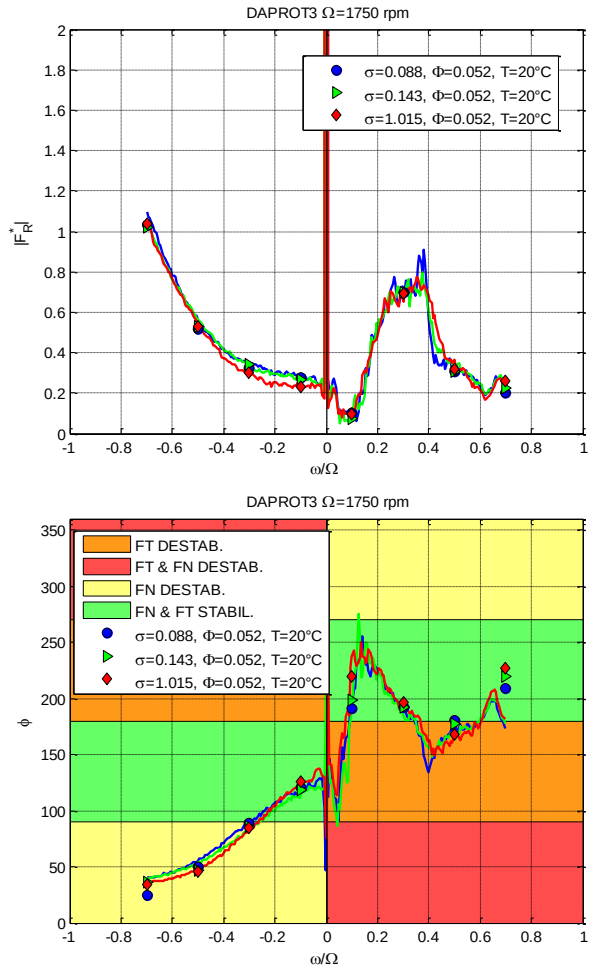

Figure 15. Effect of the cavitation number on the intensity and phase of the rotordynamic force (cold test at Φ = 0.052).

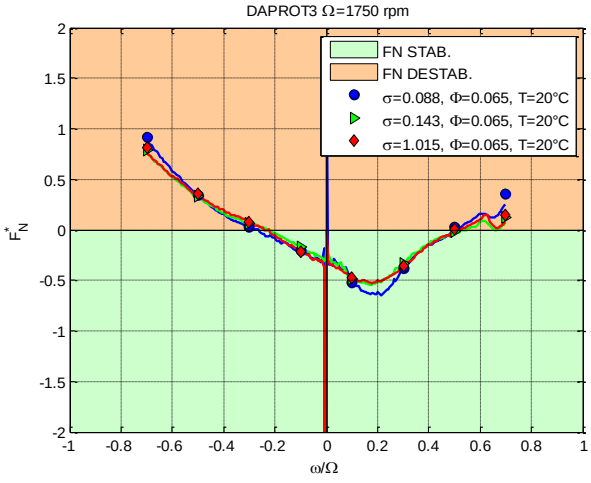

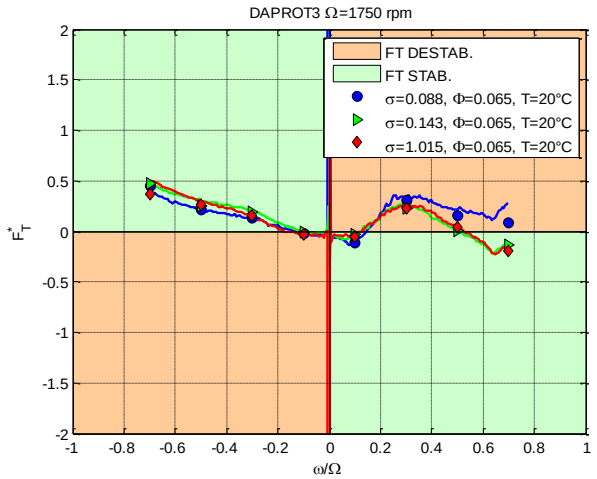

Figure 16. Effect of the cavitation number on the normal and tangential components of the rotordynamic force (cold test at Φ = 0.065).

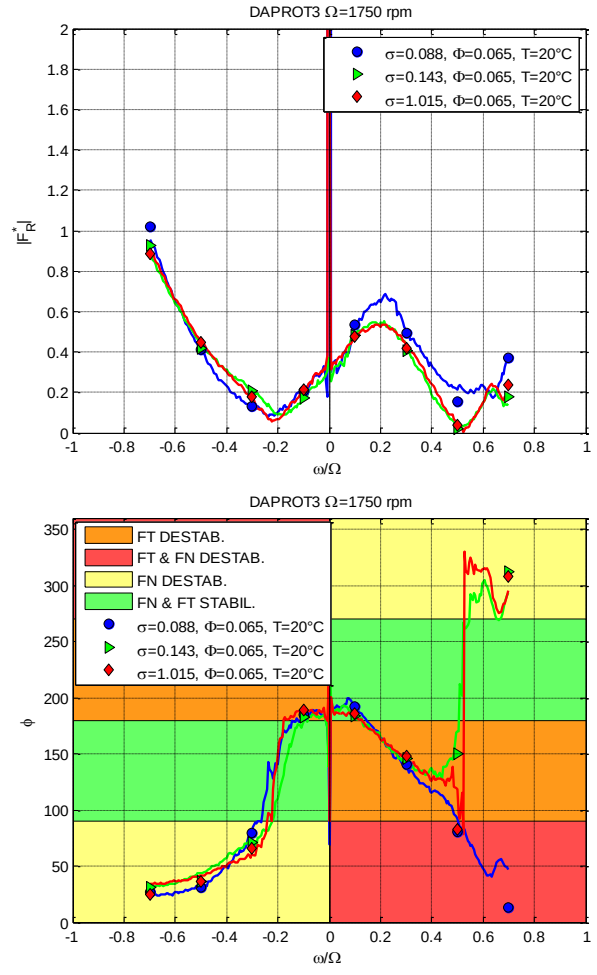

Figure 17. Effect of the cavitation number on the intensity and phase of the rotordynamic force (cold test at Φ = 0.065).

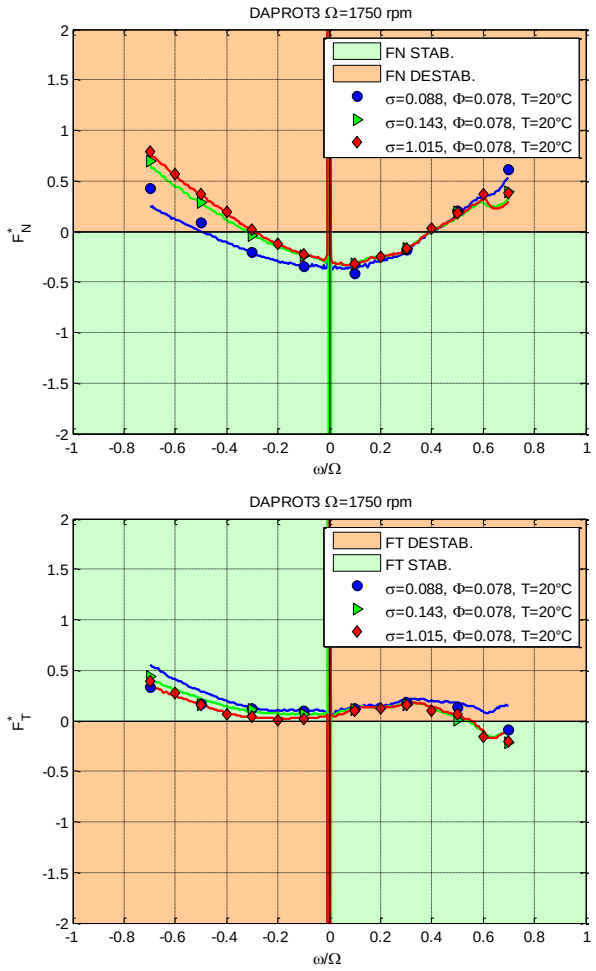

Figure 18. Effect of the cavitation number on the normal and tangential components of the rotordynamic force (cold test at $\Phi = 0.078$).

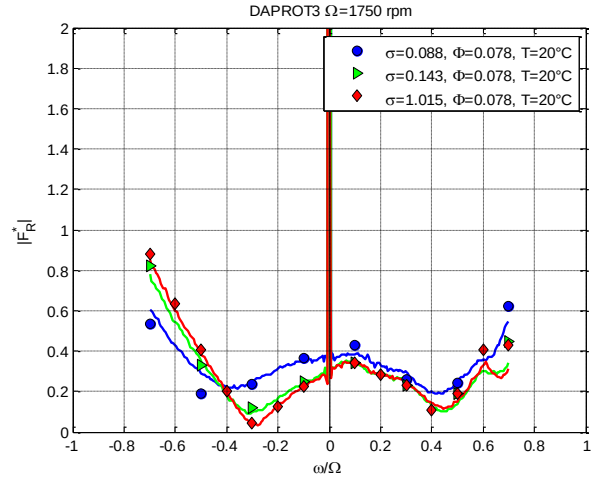

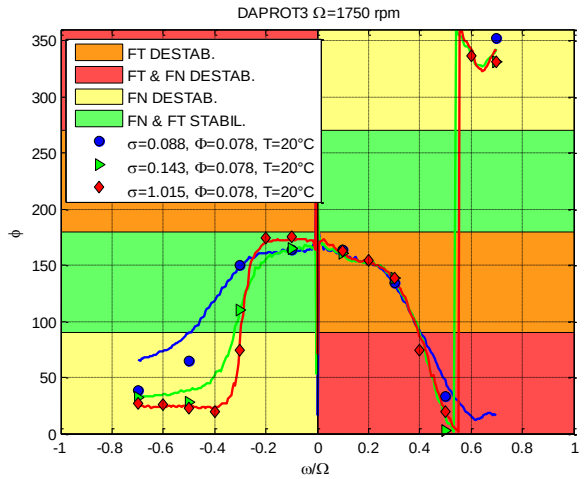

Figure 19. Effect of the cavitation number on the intensity and phase of the rotordynamic force (cold test at $\Phi = 0.078$).

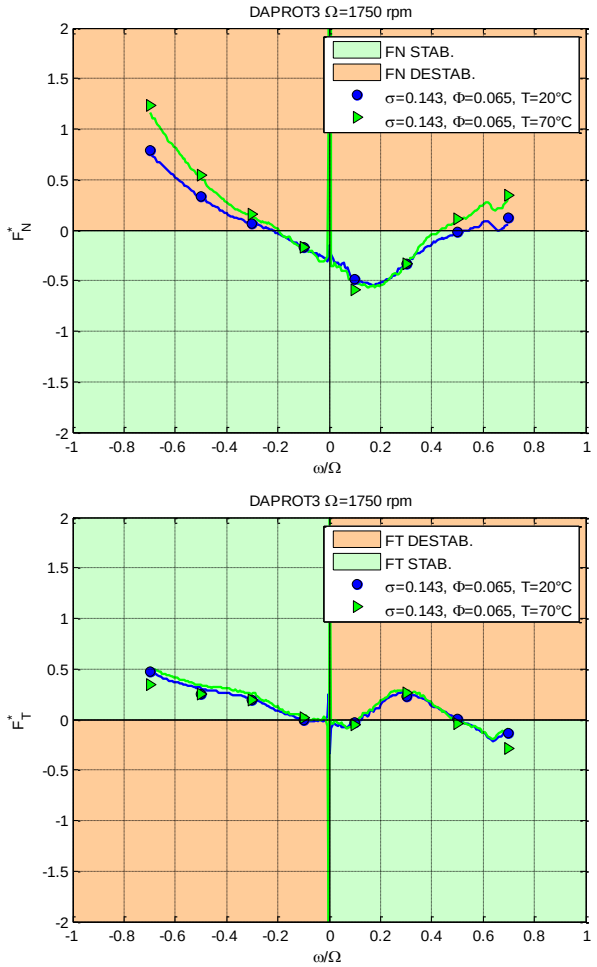

Figure 20. Effect of the fluid temperature on the normal and tangential components of the rotordynamic force (design flow coefficient, slightly cavitating).

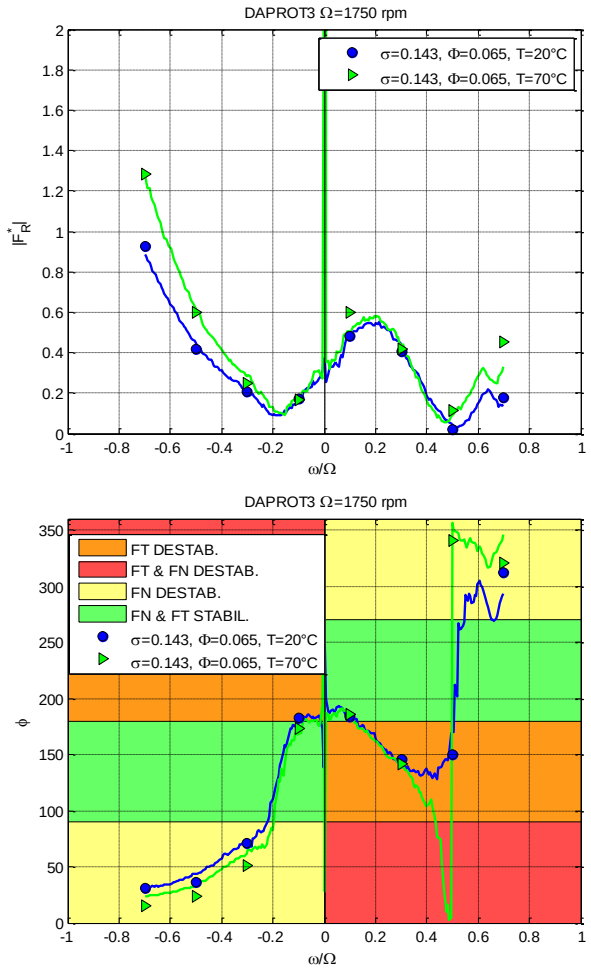

Figure 21. Effect of the fluid temperature on the intensity and phase of the rotordynamic force (design flow coefficient, slightly cavitating).

Finally, figures 20 and 21 are concerned with the effect of the fluid temperature at design flow rate under noncavitating conditions. The temperature only affects the normal component of the rotordynamic force. In particular, the magnitude of the rotordynamic force tends to increase for high temperature if the whirl ratio is higher than $\omega/\Omega = 0.5$ or lower than $\omega/\Omega = -0.2$.

Conclusions

An extensive test campaign for the characterization of the rotordynamic forces on the DAPROT3 inducer under forced whirl conditions has been conducted for several combinations of the flow coefficient, the cavitation number and the water temperature. In particular, the present paper illustrates a comparative analysis of the force measurements taken by means of a rotating dynamometer.

The continuous procedure recently developed at ALTA for the measurement of the spectral dependence of the rotordynamic forces acting on whirling impellers as functions of the whirl frequency shows good agreement with the "classical" approach. The analysis of the continuous rotordynamic force spectra allows for obtaining far more interesting and valuable information from the experimental results, by more clearly and accurately characterizing the qualitative and quantitative behavior of the rotordynamic forces on the tested impellers.

The DAPROT3 inducer has been tested at a value of the flow coefficient quite lower than the design one, characterized by the occurrence of inlet flow reversal. The effects of the flow coefficient are concerned with the intensity of the rotordynamic force (which becomes higher at lower flow coefficients) and with the translation of the curve w.r.t. the whirl frequency ratio (at lower flow coefficients the spectrum tends to shift towards higher values of the whirl ratio). This can be associated with the intensity of the flow reversal and the magnitude of the backflow prerotation induced by the leakage flow through the blade tip clearance, which increases when the flow coefficient decreases. The tip clearance flow and the rotordynamic forces experienced by the inducer are the results of the complex interaction between the flow imposed by the whirl motion of the impeller and the leakage flow caused by the differential pressure across the inducer. This interaction can be constructive (maximum) or destructive (minimum), depending on the flow conditions.

The role of cavitation seems to be directly dependent on the impeller operating point (i.e. on the flow coefficient), consequently confirming the main influence of the flowrate on rotordynamic forces on whirling impellers. More specifically, the available evidence shows that the rotordynamic force is practically independent on the cavitation number at low values of the flow coefficient. This suggests that some other effect is dominant with respect to the presence of cavitation, for example that the rotordynamic force might be mainly affected by the reverse flow. Further investigation is needed to shed better understand this phenomenon, which the authors intend to address point in further experiments.

Finally, the intensity of rotordynamic force, and in particular, its normal component, increases at higher liquid temperatures, when thermal cavitation effects become significant.

Acknowledgments

The present work has been supported by the European Space Agency under Contract No. 4000102585/10/NL/Sfe. The authors would like to express their gratitude to Dr. Giorgio Saccoccia, ESA-ESTEC, Nordwijk, The Netherlands, for his constant attention and encouragement. The authors would also like to acknowledge the valuable work of the students who have collaborated to this exciting experimental research: Andrea Bonaguidi and Ruzbeh Hadavandi. Special thanks go to L. A. Zocco & T. A. Sore from GMYS-Space.

References

1 Ehrich, F. and Childs, S. D. Self-Excited Vibrations in High Performance Turbomachinery. *Mechanical Engineering* (1984), 66-79.

2 Hergt, P. and Krieger, P. Paper 10: Radial Forces in Centrifugal Pumps with Guide Vanes. In *Proceedings of the Institution of Mechanical Engineers* (1969), SAGE Publications, 101-107.

3 Ohashi, H. and Shoji, H. Lateral Fluid Forces Acting on a Whirling Centrifugal Impeller in Vaneless and Vaned Diffuser. In *Workshop on Rotordynamic Instability*

Problems in High Performance Turbomachinery (1984), NASA Conf. Publ., 109-122.

4 Yoshida, Y., Tsujimoto, Y., Morimoto, G., Nishida, H., and Morii, S. Effects of Seal Geometry on Dynamic Impeller Fluid Forces and Moments. *ASME Journal of Fluids Engineering* (2003), 786-795.

5 Suzuki, T., Prunieres, R., Horiguchi, H., Tsukiya, T., Taenaka, Y., and Y., Tsujimoto. Measurements of Rotordynamic Forces on an Artificial Heart Pump Impeller. In *23rd IAHR Symposium* (Yokohama, Japan October 2006).

6 Jery, B. *Experimental Study of Unsteady Hydrodynamic Force Matrices on Whirling Centrifugal Pump Impellers*. Pasadena, 1987.

7 Franz, R.J. *Experimental investigation of the effect of cavitation on the rotordynamic forces on a whirling centrifugal pump impeller*. California Institute of Technology, 1989.

8 Bhattacharyya, A. *Internal Flows and Force Matrices in Axial Flow Inducers*. Pasadena, 1994.

9 Bhattacharyya, A., Acosta, A. J., Brennen, C. E., and Caughey, T. K. Rotordynamic Forces in Cavitating Inducers. *ASME Journal of Fluids Engineering* (1997), 768-774.

10 A. Pasini, L. Torre, A. Cervone, L. d'Agostino, *"Continuous Spectrum of the Rotordynamic Forces on a Four Bladed Inducer*", ASME Journal of Fluids Engineering, Vol. 133, Is. 12, December 2011

11 Torre, Lucio, Pasini, Angelo, Cervone, Angelo, and d'Agostino, Luca. Experimental Characterization of the Rotordynamic Forces on Space Rocket Axial Inducers. *ASME Journal of Fluids Engineering* (2011).

12 Torre, Lucio, Pasini, Angelo, Cervone, Angelo, Pecorari, Luca, and Milani, Andrea. Rotordynamic Forces on a Three Bladed Inducer. In *Space Propulsion Conference* (San Sebastian, Spain 2010).

13 Pace, G., Pasini, A., Torre, L., Valentini, D., and d'Agostino, L. The Cavitating Pump Rotordynamic Test Facility at ALTA S.p.A.: Upgraded Capabilities of a Unique Test Rig. In *Space Propulsion Conference* (Bordeaux,France 2012).

14 Rapposelli, E., Cervone, A., and d'Agostino, L. A New Cavitating Pump Rotordynamic Test Facility. In *JPC, AIAA Joint Propulsion Conference and Exhibit* (Indianapolis, USA 2002).

15 d'Agostino, L., Torre, L., Pasini, A., Baccarella, D., Cervone, A., and Milani, A. A Reduced Order Model for Preliminary Design and Performance Prediction of Tapered Inducers: Comparison with Numerical Simulations. In *44th AIAA/ASME/SAE/ASEE Joint Propulsion Conference* (Hartford 2008).

16 Pasini, Angelo, Torre, Lucio, Cervone, Angelo, and d'Agostino, Luca. Rotordynamic Forces on a Four Bladed Inducer. In *46th AIAA/ASME/SAE/ASEE Joint Propulsion Conference* (Nashville, USA 2010).

17 Brennen, C.E. *Hydrodynamics of Pumps*. Oxford University Press, 1994.

18 Acosta, A. J. and Bowerman, R. D. An Experimental Study of Centrifugal Pump Impellers. *Trans. ASME*, 79 (1957), 1821-1831.

19 Pasini, A., Torre, L., Cervone, A., d'Agostino, L. Characterization of the Rotordynamic Forces on Tapered Axial Inducers by Means of a Rotating Dynamometer and High-Speed Movies. In *WIMRC 3rd International Cavitation Forum* (University of Warwick, United Kingdom 2011).

20 d'Agostino, L., Torre, L., Pasini, A., and Cervone, A. On the Preliminary Design and Noncavitating Performance of Tapered Axial Inducers. *ASME Journal of Fluids Engineering*, 130, 11 (2008).